Hot Jupiters are not as lonely as we thought

Songhu Wang (sw121@iu.edu)
Indiana University
Dong-Hong Wu
Anhui Normal University
Malena Rice
Yale University https://orcid.org/0000-0002-7670-670X

Physical Sciences - Article

Keywords:

Posted Date: May 9th, 2022

DOI: https://doi.org/10.21203/rs.3.rs-1627615/v1

Hot Jupiters are not as lonely as we thought

Dong-Hong Wu[1,2], **Malena Rice**[3], and **Songhu Wang**[*4]

[1]Department of Physics, Anhui Normal University, Wuhu Anhui, 241000, PR, China

[2]School of Astronomy and Space Science and Key Laboratory of Modern Astronomy and Astrophysics in Ministry of Education, Nanjing University, Nanjing 210093, China

[3]Department of Astronomy, Yale University, New Haven, CT 06511, USA

[4]Department of Astronomy, Indiana University, Bloomington, IN 47405, USA

[*]Corresponding author: [sw121@iu.edu]

The first discovered extrasolar worlds – giant, "hot Jupiter" planets orbiting remarkably close to their parent stars [1, 2] – came as a surprise to solar-system-centric models of planet formation [3], prompting the development of new theories to produce these unexpected planets [4]. The striking dearth of observed nearby planetary companions to hot Jupiters ($\sim 2\%$ [5]) has been widely quoted as evidence in support of high-eccentricity tidal migration: a framework in which hot Jupiters form further out in their natal protoplanetary disks before being thrown inward, stripping systems of any close-in planetary companions [6, 7, 8, 9, 10, 11]. By contrast, we demonstrate through a search for transit timing variations across the full four-year *Kepler* dataset that at minimum 13% of hot Jupiters have a nearby planetary companion. This subset of hot Jupiters must have a quiescent formation history such that they were able to retain nearby companions. We also demonstrate a ubiquity of nearby planetary companions to warm Jupiters, indicating that warm Jupiters typically form quiescently. We conclude with a new paradigm for the formation of short-period gas giants that is consistent with all current lines of evidence, in which $\gtrsim 13\%$ of hot Jupiters form *in situ* and the other $\lesssim 87\%$ undergo high-eccentricity migration.

The longest-standing puzzle in the study of exoplanets concerns how hot Jupiters – Jovian-sized exoplanets orbiting exceedingly close to their host stars – form and evolve [4]. Theoretical views on hot Jupiter formation largely fall into one of the following two main frameworks:

1. Dynamical high-eccentricity migration, in which cold Jupiters are launched to highly eccentric orbits through planet-planet scattering [12, 7], Lidov–Kozai cycling [8, 9], or secular interactions [10, 11]) followed by tidal friction. These dynamically hot processes violently deliver giant planets to their current orbits, leaving them isolated.

2. Formation via quiescent mechanisms [13, 14, 15, 16]. These processes are dynamically cool, allowing nearby planetary companions to remain in the system.

Previous population studies have demonstrated that hot Jupiters are rarely accompanied by nearby planetary companions analogous to those commonly observed in compact *Kepler* multi-planet systems (typically with period ratio $P'/P \sim 1.5 - 4$ and radius $R_{\rm p} \sim 1 - 4R_{\oplus}$). This conclusion has been drawn based on a series of non-detections from Doppler velocimetric data [17], direct photometric searches for additional transiting planets in known hot Jupiter systems [18, 19, 20], and searches for aperiodic transits of detected hot Jupiters ("transit timing variations", or TTVs) induced by interactions with nearby companions [18, 21].

Recently, however, a few hidden nearby planetary companions to hot Jupiters have begun to emerge. These companions have become possible to detect through extreme precision photometric observations from the space (e.g. WASP-47 [22]; Kepler-730 [23]; TOI-1130 [24]), as well as through dedicated radial velocity (RV) follow-up measurements of known transiting hot Jupiters (WASP-148 [25]). These new discoveries provide strong evidence that at least some hot Jupiters form through quiescent mechanisms, while simultaneously suggesting that hot Jupiters' nearby low-mass planetary companions, which may lie below the detection limits of past surveys, may be more common than previously thought.

In this paper, we analyze TTVs across the full 17 quarters of *Kepler* data to estimate the occurrence rate of short-period gas giants with nearby planetary companions. A similar analysis of the first six quarters of *Kepler* data previously found no significant TTV signals among observed hot Jupiters [18]. By contrast, our search across the complete *Kepler* dataset reveals the presence of TTV signals for two hot Jupiters, as well as 14 warm Jupiters. Combining these new detections with an analysis of the underlying detection biases and completeness of the TTV method, we demonstrate that a minimum of 13% of hot Jupiter systems host at least one nearby planetary companion – a significant increase over previous findings that suggest a nearby companion rate of only $\sim 2\%$ for hot Jupiters [5]. We also show that majority of warm Jupiters host a nearby planetary companion, indicating a predominantly quiescent warm Jupiter formation mechanism.

Synthesizing these two results, we conclude with a new framework for hot and warm Jupiter formation that accounts for these elevated companion rates together with all previous observational constraints.

Results

Sample Selection

We searched the complete 17-quarter *Kepler* dataset for TTV signals observed across the full sample of validated, transiting Jupiter-sized planets ($8R_\oplus \leqslant R_p \leqslant 16R_\oplus$) with orbital periods between $P = 1-300$ days around F-, G-, and K-type main sequence stars. In total, our sample included 101 validated *Kepler* Jupiter candidates from *Kepler* DR25 (see Online Methods for sample selection details). We note that our final results depend very little on the precise sample boundaries on the Jupiters' radius, orbital period, stellar temperature, and stellar surface gravity.

TTV Pre-Processing

We adopted transit times from two previous studies [26, 27], taking the most recent available estimate for transits included in both catalogues. We removed individual transit-time measurements that are flagged as outliers in [26], since they could lead to both false-negative and false-positive detections. Then, we re-fitted the outlier-free transit mid-times using a linear model and re-calculated the TTVs as the deviation of the observed transit mid-times from the linear orbital ephemeris.

TTV Detection & Validation

We applied three previously established TTV detection techniques to our sample in search of systems with (1) excess scatter based on the modified χ^2 [28], (2) correlated variations based on the "alarm" $\mathcal{A}$ score [29], or (3) periodic signals based on the Lomb–Scargle periodogram [30] in their TTV measurements (see Online Methods for details). Each Jupiter that passed any of these three tests was identified as showing statistically significant TTVs, resulting in a set of 23 initial TTV candidates.

To validate the identified TTVs, we then determined whether the TTVs of any candidates could have instead been caused by systematics or astrophysical sources other than planetary companions: namely, variations associated with stellar spots, sampling aliases, or perturbations from stellar companions. We also excluded systems whose TTVs are believed to be caused by very distant planetary companions (instead of nearby planetary companions; see Online Methods for the TTV validation details). In total, we validated 16 out of the 23 initially identified TTV signals, demonstrating that they are most consistent with an origin from a nearby planetary companion. These systems are shown in Figure 1.

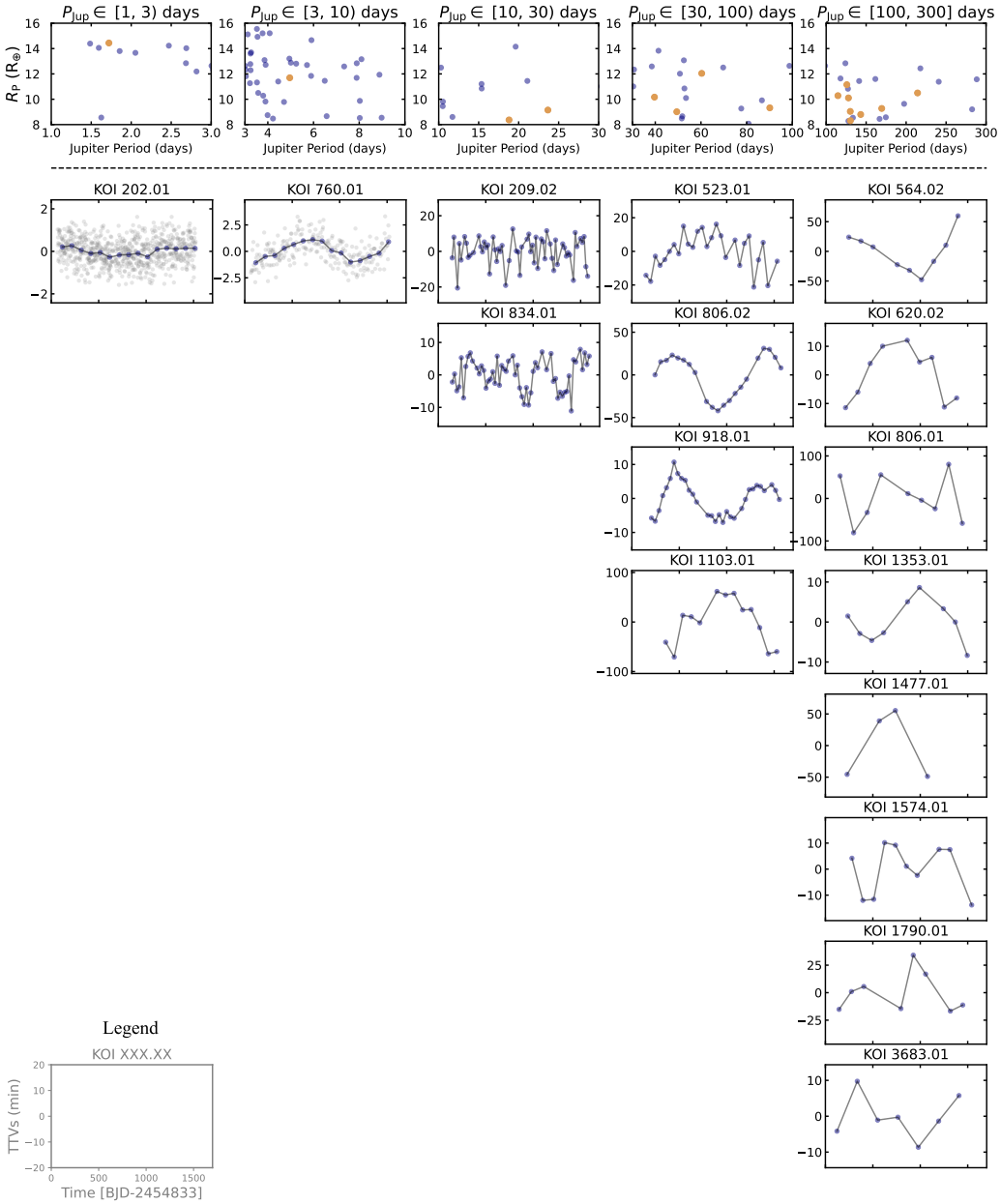

Figure 1: TTV signals for the observed sample, broken into logarithmically spaced bins. The top row shows where each system with TTVs lies in period-radius space, while the remaining panels show the observed TTVs. The legend is provided in the lower left corner for reference. The x-axis of each panel spans the full time range of *Kepler* primary mission observations, with the same range shown for each vertical column.

Table 1: Summary of results from our full analysis of *Kepler* TTVs.

Period Bins	$1.0 \leqslant P < 3.0$	$3.0 \leqslant P < 10$	$10 \leqslant P < 30$	$30 \leqslant P < 100$	$100 \leqslant P \leqslant 300.0$	Reference
# of Jupiters	10	40	10	19	22	*Kepler* DR25, Observation
# of Jupiters with TTVs	1	1	2	4	8	This work, Observation
P(TTVs|Jupiters)	$10.0\% \pm 10.0\%$	$2.5\% \pm 2.5\%$	$20.0\% \pm 10.0\%$	$21.1\% \pm 10.5\%$	$36.4\% \pm 9.1\%$	This work, Observation
P(TTVs|Nearby Companions)	$26.0\% \pm 2.8\%$	$33.5\% \pm 3.0\%$	$40.5\% \pm 3.2\%$	$43.5\% \pm 3.4\%$	$48.0\% \pm 3.3\%$	This work, Simulation
P(Nearby Companions|Jupiters)	$\mathbf{38.8\% \pm 37.6\%}$	$\mathbf{8.0\% \pm 7.4\%}$	$\mathbf{49.6\% \pm 25.7\%}$	$\mathbf{50.4\% \pm 23.7\%}$	$\mathbf{74.9\% \pm 20.0\%}$	**This work, Key Result**
	$\mathbf{13\% \pm 7\%}$		$\mathbf{63\% \pm 14\%}$			
# of Jupiters with detected transiting companions	0	1	2	3	3	*Kepler* DR25, Observation
Expected # of Jupiters with detected transiting companions	2 ± 1	2 ± 1	2 ± 1	2 ± 1	2 ± 1	This work, Simulation

Our TTV detections are in excellent agreement with previous findings that also used the full 17 quarters of *Kepler* data to identify significant TTV signals [26]. We verified that the absence of TTV detections for hot Jupiters in earlier work, which incorporated only six quarters of *Kepler* data, results from the differing temporal baselines used in each study [18] (See Online Methods for the details of our comparison with previous studies).

TTV Rate for *Kepler* Jupiters

To determine the fraction of *Kepler* Jupiters with measured TTVs as a function of their orbital period, we divided the 101 *Kepler* Jupiter samples into five logarithmically spaced period bins between $1 - 300$ days, and we calculated the fraction P(TTVs|Jupiters) of Jupiters with detected TTVs in each bin. The resulting fractions are provided in Table 1 and panel **B** of Figure 2, where the errors are given as binomial uncertainties. The number of Jupiter-sized planets is also provided for each period bin in Table 1, together with the number of those planets with detected TTVs. As shown in panel **B** of Figure 2, we find that TTVs are significantly more common in warm Jupiter systems than in hot Jupiter systems.

TTV Biases

To contextualize our findings, we next evaluated the detection sensitivity of the TTV technique to Jupiters' nearby companions P(TTVs|Nearby Companions). For a given planetary perturber mass m', eccentricity e', and period ratio P'/P, the expected TTV amplitudes are larger for Jupiters with longer orbital periods, with signal-to-noise ratio

$$\mathrm{SNR_{TTV}} \sim P^{5/6} \frac{m'}{M_*} f\left(\frac{P'}{P}, e'\right) \left(\frac{R_\mathrm{p}}{R_*}\right)^{3/2}. \quad (1)$$

Since $\mathrm{SNR_{TTV}} \sim P^{5/6}$, all else equal, *TTV measurements for hot Jupiters should have a lower SNR than analogous measurements of warm Jupiters.* Therefore, the low rate of detected hot-Jupiter TTVs from the *Kepler* dataset may result in part from this detection bias.

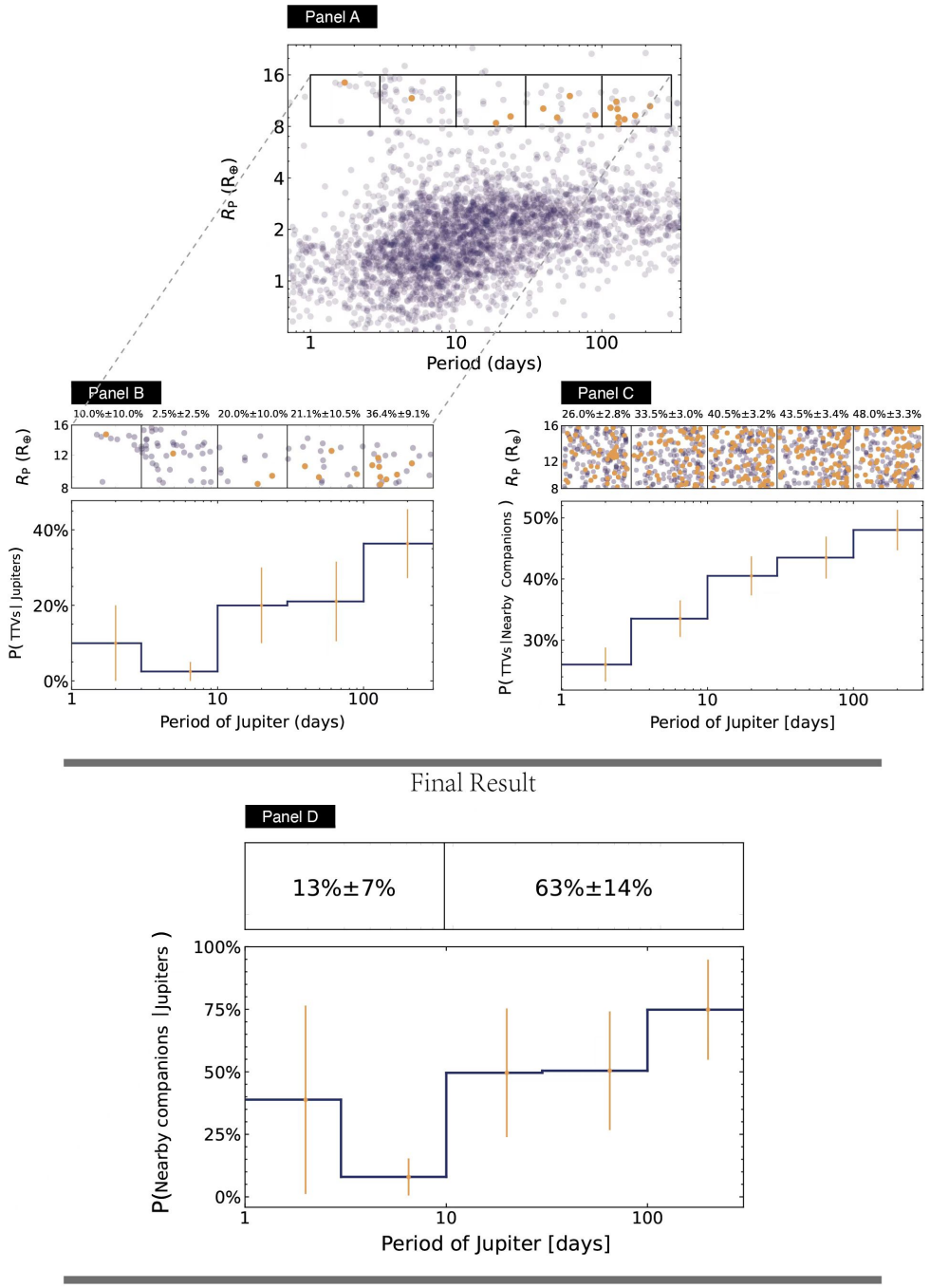

Figure 2: Summary of the observed *Kepler* TTV rates, compared with simulated recovery rates to provide a final occurrence rate of nearby companions to hot and warm Jupiters. *Panel A:* Our full sample in period-radius space, shown in the context of confirmed planets. *Panel B:* Distribution of systems with Jupiter-sized planets that show significant TTVs. *Panel C:* Simulated recovery rate of hot Jupiters with observed TTVs. *Panel D:* Final combined result for the occurrence rate of nearby companions to Jupiter-sized planets as a function of orbital period.

Detectability: Injection-Recovery Tests

Given the expected bias against observing TTVs in hot Jupiter systems, we next examined our detection completeness through a series of injection-recovery tests. For each of the five logarithmically spaced period bins used to determine the TTV rate of *Kepler* Jupiters, we generated a set of 200 trial Jupiters around solar-mass stars ($M_* = 1.0$ $M_\odot$). The Jupiters' orbital periods were randomly drawn from a uniform distribution, and planetary radii were randomly drawn from the *Kepler* DR25 Jupiter radius distribution ($8R_\oplus \leqslant R_p \leqslant 16R_\oplus$). Planetary radii were then converted to planet masses based on a mass-radius relation [31].

For each trial Jupiter system, we injected a nearby planet with a period ratio randomly drawn from the range spanned by *Kepler* multi-planetary systems (typically with $P'/P < 4.0$). We placed the injected planet on a circular orbit at a low mutual inclination $i_{\rm mut} = 0 \pm 1^\circ$. Both interior and exterior perturbers were considered. We then generated transit mid-times of each trial Jupiter by integrating the systems over a span of $1,500$ days using the `TTVFast` code [32]. These transit mid-times were fed into our TTV detection pipeline to compute the fraction of trial Jupiters P(TTVs|Nearby Companions) showing detectable TTVs induced by the injected perturbing planets. We repeated this process 100 times for each period bin, and, using the standard deviation of the detection completeness across these 100 trials, we found that the TTV recovery rates are stable at the 3% level.

We ultimately found that the TTV detectability increases with the orbital period of the transiting Jupiters (See panel **C** of Figure 2 and Table 1), in agreement with our analytic conclusion (Equation 1). For our two shortest-period bins of hot Jupiters ($P < 10$ days), only 30% of the injected TTVs were identified successfully. This result reaffirms that the dearth of detected hot-Jupiter TTVs in previous studies likely results in part from detection biases. 44% of the injected TTVs were recovered in warm Jupiter systems, indicating a higher but still incomplete recovery rate.

Implications for Nearby Planet Occurrence

Finally, we estimated the intrinsic fraction of Jupiters with nearby companions P(Nearby Companions|Jupiters) by dividing our newly constrained *Kepler* TTV rates P(TTVs|Jupiters) by our TTV detection completeness P(TTVs|Nearby Companions). This result is provided in Table 1 and shown in panel **D** of Figure 2. We ultimately find that $\gtrsim 13 \pm 7\%$ of hot Jupiters have nearby planetary companions, while majority of warm Jupiters ($\gtrsim 63 \pm 14\%$) have nearby planetary companions. Both of these values are lower limits: that is, additional perturbers may exist that are too low-mass or have a period ratio P'/P too large for our current detection limits [33]. Our results demonstrate a higher fraction of both hot and warm Jupiters with nearby

companions than has been found in previous studies [18, 19].

Comparison to the Transit Detection Rate

Next, we examined whether these Jupiters' nearby companions should typically transit their host stars, and, correspondingly, whether these companions should have been detectable in the *Kepler* dataset. We calculated the expected values by combining our predicted nearby companion rates with the well-constrained *Kepler* detection efficiency for low-mass planetary companions [34]. In all systems, we assumed a low mutual inclination $i_{\rm mut} = 0 \pm 1^\circ$ between the Jupiter and its nearby companion. We adopted the same parameter distributions for companions to hot and warm Jupiters.

The expected number of *Kepler* Jupiters with an additional, detectable transiting planet companion is consistent with observations within $1\,\sigma$. However, while we expected to find 2 ± 1 *Kepler* Jupiters with orbital periods between $1 - 3$ days in compact multi-transiting planetary systems, none were found. It is possible that hot Jupiters' nearby companions have either higher inclinations, smaller radii, or larger period ratios compared to warm Jupiters', making them difficult to detect. Because this is only a 2σ discrepancy, the absence of additional observed transiting companions to the hottest *Kepler* Jupiters may simply result from small-number statistics.

In conclusion, we found no compelling evidence for large mutual inclinations between *Kepler* Jupiters and their nearby companions by comparing our companion rate derived from TTVs with that from *Kepler* transit detection.

Overview of Findings

Our final results are summarized as follows:

- We detected TTVs for 16 Jupiter-sized planets in the *Kepler* dataset – including two hot Jupiters – substantially increasing the rate of observed TTVs in short-period Jovian systems.
- We demonstrated that, in addition to limitations imposed by the data's time baseline, the absence of previously observed TTV signals for *Kepler* hot Jupiters [18] may result from an observational bias. This is because the TTV technique is more sensitive to warm Jupiters' nearby planetary companions than to those of hot Jupiters.
- By correcting for TTV detection completeness, we demonstrated that a substantial fraction of hot Jupiters (at minimum $13 \pm 7\%$) have nearby planetary companions, while majority of warm Jupiters (at minimum $63 \pm 14\%$) have nearby planetary companions. Here, we define "nearby planetary companions"

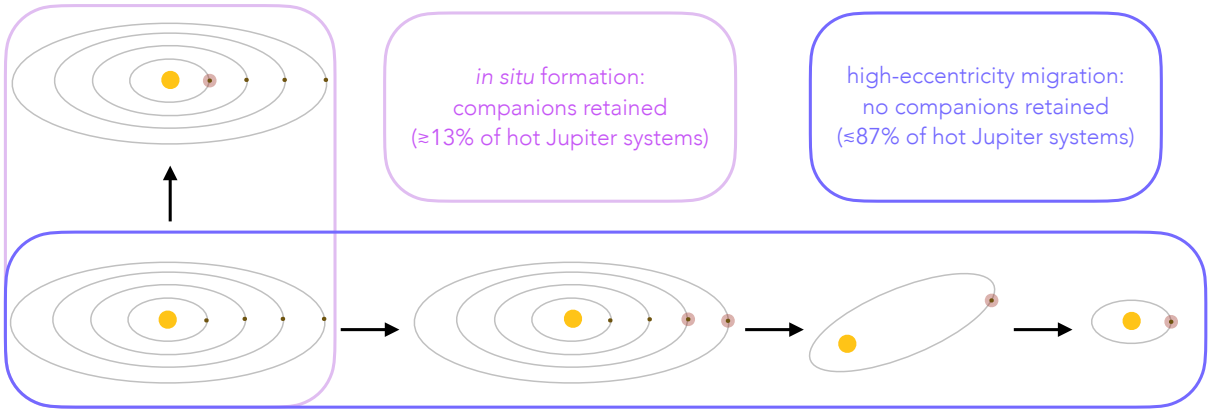

Figure 3: Key formation pathways for hot Jupiter systems. Each pathway begins from the formation of massive planetesimal cores throughout the disk. *Purple:* The inner super-Earth core experiences *in situ* runaway gas accretion to produce a hot Jupiter, and neighboring planets remain in the system. *Blue:* Two or more cores further out in the disk experience runaway gas accretion, which can initialize the high-eccentricity migration framework. The cold Jupiters may interact via planet-planet scattering, launching one gas giant onto a highly eccentric orbit and removing companions from the system. The gas giant's orbit circularizes and tidally realigns over time, producing an isolated hot Jupiter.

as companions with period ratios and radii analogous to those within *Kepler* multi-planet systems (typically with $P'/P \sim 1.5-4$ and $R_{\rm p} \sim 1-4R_{\oplus}$).

- No assumption of large mutual inclinations is required to ensure that our observed rate of nearby companions is consistent with the *Kepler* sample of transit detections.

Discussion

Combining our findings with other major demographic properties of hot and warm Jupiters [4], we put forth a new and unified framework for short-period gas giant formation that is fully consistent with all observational constraints. Our dynamical search has unveiled a higher fraction of hot and warm Jupiters with nearby planetary companions than previous results have found [18, 19, 20, 21], favoring a relatively cool dynamical history for short-period gas giants. This result indicates that at least $\sim 13\%$ of hot Jupiters and the majority of warm Jupiters — those that have successfully maintained their nearby planetary companions — must form quiescently. We propose that the other 87% of hot Jupiters formed through dynamically violent high-eccentricity migration dominantly triggered by planet-planet interaction. Our framework is summarized in Figure 3.

In our framework, super-Earth cores form throughout the natal protoplanetary disk– consistent with the high occurrence rate of super-Earths detected with *Kepler* [35]. Some of these cores are massive enough

to trigger runaway gas accretion (although the runaway process may not be needed [36]), and they become gas giants before the surrounding gas dissipates. Quiescently formed hot Jupiters ($\gtrsim 13\%$ of the total) were directly produced by this process, which allows them to retain nearby planetary companions.

After the gaseous disk has dispersed, dynamical interactions further sculpt the architecture of each system. Systems with multiple short-period giant planets may experience scattering or collisions in the inner system, which have been shown to well reproduce the observed eccentricity distribution of close-orbiting giant planets [37, 38]. In systems with massive initial protoplanetary disks, several gas giants may form further out in the disk. Planet-planet interactions, including a combination of planet-planet scattering [6] and secular mechanisms (planet-planet Kozai-Lidov cycles [39] or secular chaos [10]), send some of these gas giants to highly eccentric orbits. These orbits are then tidally circularized to produce the remaining $\lesssim 87\%$ of hot Jupiters that lack nearby companions.

A subset of isolated hot Jupiters may have instead been produced through high-eccentricity tidal migration triggered by secular Kozai-Lidov interactions with stellar companions [8]. However, hot Jupiter host stars do not have a sufficiently high rate of binary companions capable of inducing Kozai-Lidov oscillations (at most $16 \pm 5\%$ [40]) for star-planet interactions to be the dominant source of hot Jupiters. By contrast, previous work found that $70 \pm 8\%$ of hot Jupiters have an outer $1 - 13 M_J$ companion at a separation between 1 and 20 au [41, 42]. The prevalence of these distant giant companions suggests that planet-planet interactions may be a dominant contributor toward high-eccentricity migration in hot Jupiter systems. Furthermore, hot Jupiters on eccentric orbits have been found primarily around metal-rich stars, which may be more capable of producing multiple massive planets that would trigger high-eccentricity migration [43].

Our framework is also in excellent agreement with previous results demonstrating that the obliquity distribution of hot Jupiters is consistent with high-eccentricity migration as the predominant hot Jupiter formation mechanism [44]. By contrast, observed warm Jupiters in single-star systems are significantly less misaligned than their hot Jupiter counterparts (Rice et al., in prep). While hot Jupiters orbiting single stars are commonly misaligned through high-eccentricity migration, warm Jupiters in single-star systems instead have orbits aligned with the equator of their host star, as would be anticipated in our framework of quiescent formation within aligned protoplanetary disks.

Our results produce several predictions that are testable in the immediate future. For example, hot Jupiters have been found around some pre-main-sequence T Tauri stars [45, 46]. Because of the young ages of these systems, high-eccentricity migration likely could not deliver all hot Jupiters to their final short orbits around these stars. As a result, we predict that a reduced occurrence rate for hot Jupiters should be observed around

T Tauri stars as compared with main sequence stars. Furthermore, since, in our framework, a significant fraction of hot Jupiters form through planet-planet triggered high-eccentricity migration, we expect that cold-Jupiter companions to hot Jupiters should be more eccentric than cold-Jupiter companions to warm Jupiters, which did not experience a violent evolutionary history.

Our framework also solves two critical issues faced by individual formation channels. On the one hand, high-eccentricity migration alone cannot reproduce the large population of observed warm Jupiters with low eccentricities [47], which, in our framework, form via the *in situ* process. On the other hand, *in situ* formation alone cannot account for all discovered hot Jupiters– especially those with high eccentricities [48], which, in our framework, are produced by high-eccentricity migration.

In our framework, the absence of short-period gas giants in our own solar system simply reflects the solar system's formation from a relatively low-mass disk relative to those from which most discovered exoplanets formed [49]. The inner disk of the solar system likely did not contain sufficient material to form a massive core capable of triggering run-away accretion, as would be needed to produce an *in situ* hot or warm Jupiter. Less massive disks are similarly less likely to form multiple massive planets further out that would trigger high-eccentricity migration and deliver a cold gas giant to the inner system. Our solar system is therefore a natural outcome of planet formation in a lower-mass disk, representing a scaled-down version of the high-mass extrasolar systems within which hot and warm Jupiters have formed.

References

[1] Mayor, M. & Queloz, D. A Jupiter-mass companion to a solar-type star. *Nature* **378**, 355–359 (1995).

[2] Charbonneau, D., Brown, T. M., Latham, D. W. & Mayor, M. Detection of Planetary Transits Across a Sun-like Star. *ApJ* **529**, L45–L48 (2000). astro-ph/9911436.

[3] Pollack, J. B. *et al.* Formation of the giant planets by concurrent accretion of solids and gas. *Icarus* (1996).

[4] Dawson, R. I. & Johnson, J. A. Origins of Hot Jupiters. *Annual Review of Astronomy and Astrophysics* **56**, 175–221 (2018). 1801.06117.

[5] Zhu, W. & Dong, S. Exoplanet Statistics and Theoretical Implications. *ARA&A* **59** (2021). 2103.02127.

[6] Rasio, F. A. & Ford, E. B. Dynamical instabilities and the formation of extrasolar planetary systems. *Science* **274**, 954–956 (1996).

[7] Chatterjee, S., Ford, E. B., Matsumura, S. & Rasio, F. A. Dynamical Outcomes of Planet-Planet Scattering. *ApJ* **686**, 580–602 (2008). astro-ph/0703166.

[8] Wu, Y. & Murray, N. Planet Migration and Binary Companions: The Case of HD 80606b. *ApJ* **589**, 605–614 (2003). astro-ph/0303010.

[9] Naoz, S. The Eccentric Kozai-Lidov Effect and Its Applications. *ARA&A* **54**, 441–489 (2016). 1601.07175.

[10] Wu, Y. & Lithwick, Y. Secular Chaos and the Production of Hot Jupiters. *ApJ* **735**, 109 (2011). 1012.3475.

[11] Petrovich, C. Steady-state Planet Migration by the Kozai-Lidov Mechanism in Stellar Binaries. *ApJ* **799**, 27 (2015). 1405.0280.

[12] Rasio, F. A. & Ford, E. B. Dynamical instabilities and the formation of extrasolar planetary systems. *Science* **274**, 954–956 (1996).

[13] Lin, D. N. C., Bodenheimer, P. & Richardson, D. C. Orbital migration of the planetary companion of 51 Pegasi to its present location. *Nature* **380**, 606–607 (1996).

[14] Goldreich, P. & Tremaine, S. The excitation of density waves at the Lindblad and corotation resonances by an external potential. *ApJ* **233**, 857–871 (1979).

[15] Batygin, K., Bodenheimer, P. H. & Laughlin, G. P. In Situ Formation and Dynamical Evolution of Hot Jupiter Systems. *ApJ* **829**, 114 (2016). 1511.09157.

[16] Boley, A. C., Granados Contreras, A. P. & Gladman, B. The In Situ Formation of Giant Planets at Short Orbital Periods. *ApJ* **817**, L17 (2016). 1510.04276.

[17] Wright, J. T. *et al.* Ten New and Updated Multiplanet Systems and a Survey of Exoplanetary Systems. *ApJ* **693**, 1084–1099 (2009). 0812.1582.

[18] Steffen, J. H. *et al.* Kepler constraints on planets near hot Jupiters. *Proceedings of the National Academy of Sciences of the United States of America* **109**, 7982–7987 (2012). 1205.2309.

[19] Huang, C., Wu, Y. & Triaud, A. H. M. J. Warm Jupiters Are Less Lonely Than Hot Jupiters: Close Neighbors. *The Astrophysical Journal* **825**, 98 (2016). URL http://dx.doi.org/10.3847/0004-637X/825/2/98. 1601.05095.

[20] Hord, B. J. *et al.* A Uniform Search for Nearby Planetary Companions to Hot Jupiters in TESS Data Reveals Hot Jupiters Are Still Lonely. *AJ* **162**, 263 (2021). 2109.08790.

[21] Wang, X.-Y. *et al.* Transiting Exoplanet Monitoring Project (TEMP). VI. The Homogeneous Refinement of System Parameters for 39 Transiting Hot Jupiters with 127 New Light Curves. *ApJS* **255**, 15 (2021).

[22] Becker, J. C., Vanderburg, A., Adams, F. C., Rappaport, S. A. & Schwengeler, H. M. WASP-47: A Hot Jupiter System with Two Additional Planets Discovered by K2. *ApJ* **812**, L18 (2015). 1508.02411.

[23] Cañas, C. I. *et al.* Kepler-730: A Hot Jupiter System with a Close-in, Transiting, Earth-sized Planet. *ApJ* **870**, L17 (2019). 1812.08358.

[24] Huang, C. X. *et al.* TESS Spots a Hot Jupiter with an Inner Transiting Neptune. *ApJ* **892**, L7 (2020). 2003.10852.

[25] Hébrard, G. *et al.* Discovery and characterization of the exoplanets WASP-148b and c. A transiting system with two interacting giant planets. *A&A* **640**, A32 (2020). 2004.14645.

[26] Holczer, T. *et al.* Transit Timing Observations from Kepler. IX. Catalog of the Full Long-cadence Data Set. *ApJS* **225**, 9 (2016). 1606.01744.

[27] Rowe, J. F. *et al.* Planetary Candidates Observed by Kepler. V. Planet Sample from Q1-Q12 (36 Months). *ApJS* **217**, 16 (2015). 1501.07286.

[28] Mazeh, T. *et al.* Transit Timing Observations from Kepler. VIII. Catalog of Transit Timing Measurements of the First Twelve Quarters. *ApJS* **208**, 16 (2013). 1301.5499.

[29] Tamuz, O., Mazeh, T. & North, P. Automated analysis of eclipsing binary light curves - I. EBAS - a new Eclipsing Binary Automated Solver with EBOP. *MNRAS* **367**, 1521–1530 (2006). astro-ph/0601199.

[30] Scargle, J. D. Studies in astronomical time series analysis. II. Statistical aspects of spectral analysis of unevenly spaced data. *ApJ* **263**, 835–853 (1982).

[31] Chen, J. & Kipping, D. Probabilistic Forecasting of the Masses and Radii of Other Worlds. *ApJ* **834**, 17 (2017). 1603.08614.

[32] Deck, K. M., Agol, E., Holman, M. J. & Nesvorný, D. TTVFast: An Efficient and Accurate Code for Transit Timing Inversion Problems. *ApJ* **787**, 132 (2014). 1403.1895.

[33] Schlaufman, K. C. & Winn, J. N. The Occurrence of Additional Giant Planets Inside the Water-Ice Line in Systems with Hot Jupiters: Evidence Against High-Eccentricity Migration. *ApJ* **825**, 62 (2016). 1604.03107.

[34] Burke, C. J. & Catanzarite, J. Planet Detection Metrics: Per-Target Detection Contours for Data Release 25. Kepler Science Document KSCI-19111-002, id. 19. Edited by Michael R. Haas and Natalie M. Batalha (2017).

[35] Petigura, E. A., Howard, A. W. & Marcy, G. W. Prevalence of earth-size planets orbiting sun-like stars. *Proceedings of the National Academy of Sciences* **110**, 19273–19278 (2013).

[36] Suzuki, D. *et al.* Microlensing Results Challenge the Core Accretion Runaway Growth Scenario for Gas Giants. *ApJ* **869**, L34 (2018). 1812.11785.

[37] Frelikh, R., Jang, H., Murray-Clay, R. A. & Petrovich, C. Signatures of a planet–planet impacts phase in exoplanetary systems hosting giant planets. *The Astrophysical Journal Letters* **884**, L47 (2019).

[38] Anderson, K. R., Lai, D. & Pu, B. In situ scattering of warm jupiters and implications for dynamical histories. *Monthly Notices of the Royal Astronomical Society* **491**, 1369–1383 (2020).

[39] Naoz, S., Farr, W. M., Lithwick, Y., Rasio, F. A. & Teyssandier, J. Hot Jupiters from secular planet-planet interactions. *Nature* **473**, 187–189 (2011). 1011.2501.

[40] Ngo, H. *et al.* Friends of Hot Jupiters. II. No Correspondence between Hot-jupiter Spin-Orbit Misalignment and the Incidence of Directly Imaged Stellar Companions. *ApJ* **800**, 138 (2015). 1501.00013.

[41] Knutson, H. A. *et al.* Friends of hot jupiters. i. a radial velocity search for massive, long-period companions to close-in gas giant planets. *The Astrophysical Journal* **785**, 126 (2014).

[42] Bryan, M. L. *et al.* Statistics of long period gas giant planets in known planetary systems. *The Astrophysical Journal* **821**, 89 (2016).

[43] Dawson, R. I. & Murray-Clay, R. A. Giant planets orbiting metal-rich stars show signatures of planet–planet interactions. *The Astrophysical Journal Letters* **767**, L24 (2013).

[44] Rice, M., Wang, S. & Laughlin, G. Origins of hot jupiters from the stellar obliquity distribution. *The Astrophysical Journal Letters* **926**, L17 (2022).

[45] Donati, J. *et al.* A hot jupiter orbiting a 2-million-year-old solar-mass t tauri star. *Nature* **534**, 662–666 (2016).

[46] Yu, L. *et al.* A hot jupiter around the very active weak-line t tauri star tap 26. *Monthly Notices of the Royal Astronomical Society* **467**, 1342–1359 (2017).

[47] Petrovich, C. & Tremaine, S. Warm Jupiters from Secular Planet-Planet Interactions. *ApJ* **829**, 132 (2016). 1604.00010.

[48] Goldreich, P., Lithwick, Y. & Sari, R. Planet Formation by Coagulation: A Focus on Uranus and Neptune. *ARA&A* **42**, 549–601 (2004). astro-ph/0405215.

[49] Chiang, E. & Laughlin, G. The minimum-mass extrasolar nebula: in situ formation of close-in super-Earths. *MNRAS* **431**, 3444–3455 (2013). 1211.1673.

Online Methods

A. Detailed Sample Selection

Our sample includes the population of Jupiter-sized ($8R_\oplus \leqslant R_p \leqslant 16R_\oplus$) planets from the *Kepler* dataset with impact parameter $b < 0.9$. Transit parameters were drawn from *Kepler* DR25 [1], with refined stellar radii (and therefore planetary radii) from Gaia DR2 [2].

Our Jupiter sample exhibits periods from $P = 1 - 300$ days, with an upper period limit set to ensure that nearly all Jupiters produce at least 5 transiting events across the ~ 1500-day *Kepler* dataset. We restrict our sample to F-, G-, and K-type main sequence stars with stellar effective temperature $4700\,\mathrm{K} \leqslant T_{\rm eff} \leqslant 6500\,\mathrm{K}$ and surface gravity $\log g \geqslant 4.0$. Our final sample includes 101 Jupiter-sized planets.

B. TTV Search Techniques

We applied three separate methods to search for significant TTV signals, described in detail here.

Detection Method 1: Excess Scatter in TTVs

We first identified systems with TTV scatter that is larger than expected. This "excess scatter" was calculated using the modified χ^2 of TTVs of a system [3, 4], defined as:

$$\chi^2_{\rm modified} = N\frac{(\mathrm{median}(\{|\mathrm{TTV_i}|\}))^2}{\sigma^2_{\rm TTV}}, i = 1, 2, \cdots, N \quad (1)$$

where N is the number of TTV measurements and $\sigma_{\rm TTV}$ is the corresponding TTV uncertainty of each measurement. Instead of taking each individual TTV measurement into account as in the conventional χ^2 metric, $\chi^2_{\rm modified}$ uses the median value of the TTVs. This median value is less sensitive to outliers, such that $\chi^2_{\rm modified}$ is less sensitive to individual bad measurements. This provides a more robust detection for true TTV signals.

We applied a χ^2-test on $\chi^2_{\rm modified}$ and obtained the corresponding p-value for each system, where the null hypothesis corresponds to no transit mid-time deviations from a linear transit ephemeris. We identified TTVs as significant if $p < 10^{-4}$.

Detection Method 2: Correlated Variations in TTVs

The "alarm" $\mathcal{A}$ score [5] of a time series is sensitive to the correlated variations without assuming any functional shape of the variations. It is defined as:

$$\mathcal{A} = \frac{1}{\chi^2} \sum_{i=1}^{n} \left(\frac{\mathrm{TTV_{i,1}}}{\sigma_{\mathrm{TTV_{i,1}}}} + \cdots + \frac{\mathrm{TTV_{i,j}}}{\sigma_{\mathrm{TTV_{i,j}}}} + \cdots + \frac{\mathrm{TTV_{i,k_i}}}{\sigma_{\mathrm{TTV_{i,k_i}}}} \right)^2 , \tag{2}$$

where $\mathrm{TTV_{i,j}}$ is the jth TTV measurement of the ith "run", and $\sigma_{\mathrm{TTV_{i,j}}}$ is the corresponding uncertainty. A "run" is defined as a maximal series of consecutive TTVs with the same sign (compared with linear orbital ephemerides). The total number of runs is given by n, and k_i is the total number of TTV measurements in the ith run.

We determined the False Alarm Possibility (FAP) of the calculated $\mathcal{A}$ score by obtaining alarm scores for 10,000 different random permutations of the same TTV series. A TTV signal was identified as significant if the FAP of the $\mathcal{A}$ score was less than 10^{-4}.

Detection Method 3: Periodic Signals in TTVs

The $\chi^2_{\mathrm{modified}}$ and $\mathcal{A}$ tests have relatively low sensitivity to periodic TTVs with low amplitudes. In order to maximize our detection yield, we also produced a Lomb-Scargle periodogram [6] for each system. We identified the highest peak and calculated its FAP. We identified periodicities with FAP $< 10^{-4}$ as significant detections.

C. TTV Validation

In our validation process, we tested whether the observed TTVs could have been produced by sources other than nearby planets. Potential sources of spurious TTV signals include starspots, sampling aliases, distant planetary and stellar companions. We summarize our tests for each of these possibilities below.

Starspots

Spurious TTVs can be produced by the deformation of planet transits by stellar activity — in particular, starspots [7]. In addition to altering the measured transit mid-times, starspots also produce global modulations in each light curve as the host star rotates. This manifests in the *Kepler* transit photometry as a significant local slope in the system's light curve (that is, the stars' flux derivative).

Of our 23 identified TTV systems, we found that four of them (KOI 203.01, KOI 208.01, KOI 883.01, and KOI 1458.01) show correlations between their TTVs and the local slope of the light curves. The observed correlations are likely caused by starspot crossing. Two of the four excluded systems (KOI 203.01 and KOI 883.01) also have peak TTV periods (11.97 ± 0.9 days and 9.07 ± 1.3 days, respectively) that are similar to

their host stars' rotational period (12.05 days and 9.01 days, respectively). As a result, we removed these four systems from our final TTV sample. The remaining 19 TTV systems do not demonstrate any periodicities related to the host stars' rotation periods or their harmonics measured from global modulations in their *Kepler* light curves [8, 7].

Sampling Aliases

Non-astrophysical effects, such as stroboscopic sampling, can also mimic significant TTVs [9]. As a result, we checked whether our detected TTVs may arise as an alias of the *Kepler* sampling frequency. We calculated the stroboscopic periods of the measured TTVs following the methods of previous work [9]. We found that KOI 135.01 and KOI 208.01 have TTV periods (737 ± 164 days and 373 ± 25 days, respectively) near the stroboscopic periods or their harmonics (1532 days and 340 days, respectively). Therefore, we excluded these systems from our final TTV sample.

Stellar Companions

We also tested the possibility that the TTV signals are produced by a stellar companion [10]. For each system, we queried for all neighboring sources within the `SIMBAD` database [11], and we examined the projected separation, proper motion, and parallax to search for comoving companions. We adopted the same criteria for stellar companions that were outlined in previous work [12].

Ultimately, we found that none of the Jupiters with significant TTVs are located in systems with a known stellar companion. Two of our systems, KOI 523.01 and KOI 564.02, were found with projected separation within 5 pc of nearby stellar sources (2MASS J19041830+4503558 and 2MASS J19370034+4216580, respectively). No proper motion or parallax measurements have been reported for either candidate companion.

An additional stellar companion in a transiting planet system will induce TTVs via 1) gravitational perturbations between the stellar companion and the transiting planet [10] and 2) the light travel time effect induced by the movement of the host star [13]. The TTV period produced by both effects should be equivalent to the orbital period of the stellar companion. None of our detected TTV signals, with typical TTV periods of several thousand days, can be produced by stellar companions unless they are nonphysically close to the planetary host stars.

Very Distant Planetary Companions

We then checked whether each of our identified TTV signals may instead be associated with a very distant planetary companion. Distant planetary companions can be distinguished by the non-sinusoidal TTV signals that they induce.

We found that two of our detected TTVs (KOI 824.01 and KOI 1474.01) are consistent with apparent non-sinusoidal variations. Previous work found that the non-sinusoidal TTVs of KOI 824.01, a $P = 15$ day warm Jupiter, are likely caused by a $94\,M_{\rm Jup}$ companion at $a = 2.8$ AU [14], while the TTVs of KOI 1474.01, a $P = 70$ day warm Jupiter, are likely caused by a $7.3\,M_{\rm Jup}$ companion at $a = 1.7$ AU [15]. Thus, we exclude KOI 824.01 and KOI 1474.01 to ensure that all of our validated Jupiter TTVs are consistent with an origin from a *nearby* planetary companion.

Other possibilities

Lastly, we searched for the signatures of other timing effects, such as apsidal procession [16], orbital decay [17], or general relativistic effects [18]. None of these possibilities are consistent with our detected TTV signals.

D. Sensitivity of the TTV Technique to Jupiters' Companions

To contextualize our findings, we evaluated the detection sensitivity of the TTV technique to Jupiters' nearby planetary companions. In this section, we first describe the detection biases inherent to the TTV detection method through a semi-analytic approach (Section D1.). We then describe the series of injection-recovery tests used to evaluate our detection efficiency as a function of the Jupiter's orbital period (Section D2.). By accounting for the true detection sensitivity of the TTV technique, we calculated the corrective factor necessary to determine the true fraction of Jupiters with nearby planet companions.

D1. Semi-Analytic Approach

Given a transiting Jupiter with orbital period P and mass m, as well as a perturbing planet with orbital period P' and mass m' around a host star with stellar mass M_* and stellar radius R_*, the TTV amplitude $V_{\rm TTV}$ for the transiting Jupiter can be described as

$$V_{\rm TTV} \sim P\frac{m'}{M_*} f(\frac{P'}{P}, e'), \tag{3}$$

where $f(\frac{P'}{P}, e')$ is a function of the period ratio between perturbing planet and transiting Jupiter ($\frac{P'}{P}$) and the orbital eccentricity e' of the perturbing planet [19, 20]. This relation holds irrespective of whether the two planets are near mean-motion resonance. Equation 3 demonstrates that the TTV signal is proportional to the orbital period of the transiting Jupiter (P). *The longer the orbital period, the larger the TTV amplitude.*

The uncertainty of a transit mid-time $\sigma_{\rm TTV}$ is given by

$$\sigma_{\rm TTV} \sim T_{14}^{1/2} \left(\frac{R_{\rm p}}{R_*} \right)^{-3/2}, \tag{4}$$

where $R_{\rm p}/R_*$ is the radius ratio between the transiting Jupiter and the host star [19]. T_{14}, the transit duration of the Jupiter, is proportional to $P^{1/3}$ such that

$$\sigma_{\rm TTV} \sim P^{1/6} \left(\frac{R_{\rm p}}{R_*} \right)^{-3/2}. \tag{5}$$

The signal-to-noise ratio of the TTVs, therefore, has the form

$$\mathrm{SNR}_{\rm TTV} = \frac{V_{\rm TTV}}{\sigma_{\rm TTV}} \sim P^{5/6} \frac{m'}{M_*} f\Big(\frac{P'}{P}, e' \Big) \Big(\frac{R_{\rm p}}{R_*} \Big)^{3/2}, \tag{6}$$

which is consistent with the functional form derived in previous work [21].

For a given set of host star (M_* and R_*) and perturbing planet (m', e', and $\frac{P'}{P}$) properties, the SNR of observed TTVs for a transiting planet is an increasing function of its orbital period:

$$\boxed{\mathrm{SNR}_{\rm TTV} \sim P^{5/6}}. \tag{7}$$

All else equal, TTV measurements for hot Jupiters should have a lower SNR than analogous measurements of warm Jupiters.

D2. Injection-Recovery Initialization

In our injection-recovery tests, we generated a set of 200 trial Jupiters around solar-mass ($M_\star = 1.0\,M_\odot$) stars with orbital periods randomly drawn from a uniform distribution. Planetary radii were randomly drawn from the *Kepler* DR25 Jupiter radius distribution between $8R_\oplus$ and $16R_\oplus$.

We then injected a nearby planet into each trial Jupiter system. The radii and period ratios of the injected planets were randomly drawn from the distributions spanned by *Kepler* multi-planetary systems. Both interior and exterior perturbers were considered. The planetary radii were converted to masses based on a mass-radius relation [22].

All systems were initialized with the following orbital conditions:

1. Both planets are initially on circular orbits.

Table 1: KOIs with significant TTVs.

KOI	Planet Radius $[R_\oplus]$	Planet Period [days]	TTV Amplitude [min]	TTV period [days]	Detection Method
202.01	14.44	1.72	0.62	1274.44	TTV periodicity
209.02	8.37	18.80	7.65	50.69	$\chi^2_{\rm modified}$
523.01	9.01	49.4	10.28	1210.52	$\chi^2_{\rm modified}$
564.02	10.11	127.91	31.14	1236.11	$\chi^2_{\rm modified}$
620.02	9.04	130.18	8.69	1316.56	$\chi^2_{\rm modified}$
760.01	11.69	4.96	1.24	1114.52	$\mathcal{A}$ score, TTV periodicity
806.01	8.80	143.21	51.78	383.61	$\chi^2_{\rm modified}$
806.02	12.04	60.32	23.63	1016.05	$\chi^2_{\rm modified}$, $\mathcal{A}$ score
834.01	9.15	23.65	4.78	384.01	TTV periodicity
918.01	10.17	39.64	4.75	835.49	$\chi^2_{\rm modified}$, $\mathcal{A}$ score
1103.01	9.32	90.12	44.90	1068.05	$\chi^2_{\rm modified}$
1353.01	11.15	125.87	4.94	1029.73	$\chi^2_{\rm modified}$
1477.01	9.27	169.50	47.59	933.70	$\chi^2_{\rm modified}$
1574.01	10.28	114.74	8.92	560.87	$\chi^2_{\rm modified}$
1790.01	8.31	130.35	17.05	601.51	$\chi^2_{\rm modified}$
3683.01	10.50	214.31	5.65	1006.82	$\chi^2_{\rm modified}$

2. The mutual inclination $i_{\rm mut}$ between the two planet orbits follows a Gaussian distribution with expected value $\mu_{i_{\rm mut}} = 0^\circ$ and standard deviation $\sigma_{i_{\rm mut}} = 1^\circ$: $i_{\rm mut} \in \mathcal{N}(\mu = 0^\circ; \sigma = 1^\circ)$.

3. Both planets follow a uniform distribution between 0° and 360° for the longitude of the ascending node (Ω, Ω'), and the initial mean anomaly (M_0, M_0'); that is, Ω, Ω', M_0, $M_0' \in \mathcal{U}(0^\circ; 360^\circ)$.

4. The planetary system is Hill stable ($P'/P > 1.36$) [23].

We integrated each system over a span of 1,500 days, using the `TTVFast` code [24] to compute the transit mid-times. The uncertainties of the transit mid-times ($\sigma_{\rm TTV}$) were randomly drawn from a uniform distribution between $0 - 2$ min, which is similar to the typical TTV uncertainties measured from the *Kepler* dataset [4]. Then, we quantified the detection completeness in each period bin by calculating the fraction of injected TTVs that were identified as significant, employing the same procedures applied to the injection-free *Kepler* dataset (see Section B of the Online Methods).

We repeated this process 100 times for each period bin. The final TTV detection completeness in each period bin was calculated as the median value of the detection completeness of the 100 groups, and the 1σ errors were calculated as the corresponding standard deviations.

E. Comparison with Previous TTV Studies

For the 84 Jupiter candidates included in both our analysis and a previous *Kepler* TTV study [4], we obtain

the same TTV identification on 81 of them. We identified KOI 209.02 as a significant TTV target based on its excess scatter ($\chi_{\rm modified} = 163.33$,with $p < 1 \times 10^{-6}$), while it was undetected in the previous work [4]. Previous study confirmed that KOI 209.02's TTVs is caused by additional transiting planet in the same system [25]. Two candidates identified as significant TTV targets in previous work, KOI 1335.01 and KOI 1552.01, did not pass any of the detection criteria that we set, nor the thresholds of the previous work; they were instead identified in previous work based on visual inspection [4]. To maintain objectivity in our results, we do not consider any candidates that are not identified by our quantitative metrics.

None of our candidates were recovered by analogous work that included only six quarters of *Kepler* data and a much smaller Jupiter sample [26]. This work detected TTV signals for five Jupiter-sized planetary candidates; four of them (KOI 190.01, KOI 1003.01, KOI 1177.01 and KOI 1382.01), however, were later flagged as false positives in *Kepler* DR25. Although KOI 137.02 (Kepler-18c) shows a robust TTV signal, it was later confirmed to be a super-Earth [27]. All five of these systems were therefore excluded from our initial sample of 101 *Kepler* Jupiters.

To prove that our candidates were newly recovered due to the longer temporal baseline of our dataset, we applied our detection pipeline to conduct the same analysis using only the first six quarters of *Kepler* data. We confirmed the key result that no hot Jupiters show robust TTVs in this less extended dataset. From this analysis, we also identified four warm-Jupiter systems (KOI 209.02, KOI 806.02, KOI 918.01 and KOI 1474.01) with significant TTV signals. All four targets were unreported in the previous search because all have orbital periods longer than the upper period boundary set by that work ($P = 15.8$ days) [26].

F. Comparison with Observed Transiting Companions

To compare our results with transit detection constraints from *Kepler*, we conducted an additional set of injection tests. We randomly assigned nearby companions to the 101 Jupiter systems in our full sample, with the companion probability set by our observed fraction of nearby companions in each period bin (see Table 1 in the main text). Injected companions were added with the following constraints:

1. The mutual inclination between the companion and the Jupiter was randomly selected from a Gaussian distribution $i_{\rm mut} = 0 \pm 1^{\circ}$.

2. The planetary radius of the companion was randomly selected from the observed distribution of planets with $R_p < 8\ R_{\oplus}$ in *Kepler* multiplanet systems.

3. The period ratio between the companion and the Jupiter was randomly selected from the *Kepler* period ratio distribution, with values $P'/P < 4$. To ensure Hill stability, we set a lower limit $P'/P > 1.36$.

A planet on a circular orbit is observed to transit its host star if it has an orbital inclination $90^{\circ} -$

$\arctan(R_\star/a) < i < 90^\circ + \arctan(R_\star/a)$, where a perfectly edge-on orbit has $i = 90^\circ$. The orbital inclination of the Jupiter was randomly chosen from a uniform distribution between the minimum and maximum value of this transiting range, while the orbital inclination of the companion was chosen with $i_{\rm mut} = 0 \pm 1^\circ$ relative to the Jupiter.

Then, we determined for each system whether the injected companion (if present) falls within the expected detection limits of *Kepler*. If the planet falls outside of the inclination limits of a transiting planet, then it is not detectable. The completeness fraction for a given planet radius and orbital period is quantified as $f_{\rm tot} = f_{\rm S/N}(R,P) f_{\rm vet}(R,P)$, where $f_{\rm S/N}(R,P)$ is the *Kepler* detection efficiency, while $f_{\rm vet}(R,P)$ is the vetting completeness. The fraction $f_{\rm S/N}(R,P)$ has been constrained using KeplerPORTS [28], while we calculated $f_{\rm vet}(R,P)$ on a 100×100 grid of logarithmically spaced radii and logarithmically spaced orbital periods following the methods of previous work [29]. The exact value of $f_{\rm vet}(R,P)$ for each system was then interpolated from this grid.

Based on this analysis, we found that 2 ± 1 Jupiters in each period bin should have detected transiting companions. This is consistent with our TTV results for all bins except the shortest-period systems (1.0 days $\leqslant P <$ 3.0) days, where we found a 2σ disrepancy. This suggests that nearby companions to the hottest Jupiters may have relatively high inclinations, small radii, or large period ratios by comparison with companions to warm Jupiters.

Code availability

All codes used in this study will be publicly available before publication.

Data availability

All data generated or analyzed during this study are publicly available as part of the *Kepler* dataset.

References

[1] Thompson, S. E. *et al.* Planetary Candidates Observed by Kepler. VIII. A Fully Automated Catalog with Measured Completeness and Reliability Based on Data Release 25. *ApJS* **235**, 38 (2018). 1710.06758.

[2] Berger, T. A. *et al.* The Gaia-Kepler Stellar Properties Catalog. I. Homogeneous Fundamental Properties for 186,301 Kepler Stars. *AJ* **159**, 280 (2020). 2001.07737.

[3] Mazeh, T. *et al.* Transit Timing Observations from Kepler. VIII. Catalog of Transit Timing Measurements of the First Twelve Quarters. *ApJS* **208**, 16 (2013). 1301.5499.

[4] Holczer, T. *et al.* Transit Timing Observations from Kepler. IX. Catalog of the Full Long-cadence Data Set. *ApJS* **225**, 9 (2016). 1606.01744.

[5] Tamuz, O., Mazeh, T. & North, P. Automated analysis of eclipsing binary light curves - I. EBAS - a new Eclipsing Binary Automated Solver with EBOP. *MNRAS* **367**, 1521–1530 (2006). astro-ph/0601199.

[6] Scargle, J. D. Studies in astronomical time series analysis. II. Statistical aspects of spectral analysis of unevenly spaced data. *ApJ* **263**, 835–853 (1982).

[7] Mazeh, T., Perets, H. B., McQuillan, A. & Goldstein, E. S. Photometric amplitude distribution of stellar rotation of kois– indication for spin-orbit alignment of cool stars and high obliquity for hot stars. *The Astrophysical Journal* **801**, 3 (2015). URL https://doi.org/10.1088/0004-637x/801/1/3.

[8] McQuillan, A., Mazeh, T. & Aigrain, S. Stellar rotation periods of the kepler objects of interest: A dearth of close-in planets around fast rotators. *The Astrophysical Journal* **775**, L11 (2013). URL https://doi.org/10.1088/2041-8205/775/1/l11.

[9] Szabó, R. *et al.* Multiple planets or exomoons in Kepler hot Jupiter systems with transit timing variations? *A&A* **553**, A17 (2013). 1207.7229.

[10] Borkovits, T., Csizmadia, S., Forgács-Dajka, E. & Hegedüs, T. Transit timing variations in eccentric hierarchical triple exoplanetary systems. I. Perturbations on the time scale of the orbital period of the perturber. *A&A* **528**, A53 (2011). 1010.0884.

[11] Wenger, M. *et al.* The simbad astronomical database-the cds reference database for astronomical objects. *Astronomy and Astrophysics Supplement Series* **143**, 9–22 (2000).

[12] El-Badry, K., Rix, H.-W. & Heintz, T. M. A million binaries from gaia edr3: sample selection and validation of gaia parallax uncertainties. *Monthly Notices of the Royal Astronomical Society* **506**, 2269–2295 (2021).

[13] Irwin, J. B. The Determination of a Light-Time Orbit. *ApJ* **116**, 211 (1952).

[14] Masuda, K. Eccentric Companions to Kepler-448b and Kepler-693b: Clues to the Formation of Warm Jupiters. *AJ* **154**, 64 (2017). 1706.04990.

[15] Dawson, R. I. *et al.* LARGE ECCENTRICITY, LOW MUTUAL INCLINATION: THE THREE-DIMENSIONAL ARCHITECTURE OF a HIERARCHICAL SYSTEM OF GIANT PLANETS. *The Astrophysical Journal* **791**, 89 (2014). URL https://doi.org/10.1088/0004-637x/791/2/89.

[16] Ragozzine, D. & Wolf, A. S. Probing the interiors of very hot jupiters using transit light curves. *The Astrophysical Journal* **698**, 1778 (2009).

[17] Patra, K. C. *et al.* The apparently decaying orbit of WASP-12b. *The Astronomical Journal* **154**, 4 (2017). URL https://doi.org/10.3847/1538-3881/aa6d75.

[18] Iorio, L. Classical and relativistic node precessional effects in WASP-33b and perspectives for detecting them. *Ap&SS* **331**, 485–496 (2011). 1006.2707.

[19] Holman, M. J. & Murray, N. W. The Use of Transit Timing to Detect Terrestrial-Mass Extrasolar Planets. *Science* **307**, 1288–1291 (2005). astro-ph/0412028.

[20] Agol, E., Steffen, J., Sari, R. & Clarkson, W. On detecting terrestrial planets with timing of giant planet transits. *MNRAS* **359**, 567–579 (2005).

[21] Steffen, J. H. Sensitivity bias in the mass-radius distribution from transit timing variations and radial velocity measurements. *MNRAS* **457**, 4384–4392 (2016). 1510.04750.

[22] Chen, J. & Kipping, D. Probabilistic Forecasting of the Masses and Radii of Other Worlds. *ApJ* **834**, 17 (2017). 1603.08614.

[23] Gladman, B. Dynamics of systems of two close planets. *Icarus* **106**, 247–263 (1993). URL https://www.sciencedirect.com/science/article/pii/S0019103583711693.

[24] Deck, K. M., Agol, E., Holman, M. J. & Nesvorný, D. TTVFast: An Efficient and Accurate Code for Transit Timing Inversion Problems. *ApJ* **787**, 132 (2014). 1403.1895.

[25] Wu, D.-H., Wang, S., Zhou, J.-L., Steffen, J. H. & Laughlin, G. TTV-determined Masses for Warm Jupiters and Their Close Planetary Companions. *AJ* **156**, 96 (2018). 1807.02217.

[26] Steffen, J. H. *et al.* Kepler constraints on planets near hot Jupiters. *Proceedings of the National Academy of Sciences of the United States of America* **109**, 7982–7987 (2012). 1205.2309.

[27] Cochran, W. D. *et al.* Kepler-18b, c, and d: A System of Three Planets Confirmed by Transit Timing Variations, Light Curve Validation, Warm-Spitzer Photometry, and Radial Velocity Measurements. *ApJS* **197**, 7 (2011). 1110.0820.

[28] Burke, C. J. & Catanzarite, J. Planet Detection Metrics: Per-Target Detection Contours for Data Release 25. Kepler Science Document KSCI-19111-002, id. 19. Edited by Michael R. Haas and Natalie M. Batalha (2017).

[29] Mulders, G. D., Pascucci, I., Apai, D. & Ciesla, F. J. The exoplanet population observation simulator. i. the inner edges of planetary systems. *The Astronomical Journal* **156**, 24 (2018). URL https://doi.org/10.3847/1538-3881/aac5ea.

Acknowledgements

We thank Greg Laughlin, Eric Ford, Fred Adams, Kevin Schlaufman, Bonan Pu, Jiayin Dong, and Beibei Liu for insightful discussions. We thank Xian-Yu Wang and the Metrics for polishing figures. D.W. is supported by the National Natural Science Foundation of China (NSFC) (grant No. 12103003), the funding from Key Laboratory of Modern Astronomy and Astrophysics in Ministry of Education, Nanjing University, and the Doctoral research start-up funding of Anhui Normal University. M.R. is supported by the National Science Foundation Graduate Research Fellowship Program under Grant Number DGE-1752134. This research has made use of the NASA Exoplanet Archive, which is operated by the California Institute of Technology, under contract with the National Aeronautics and Space Administration under the Exoplanet Exploration Program.

Author Contributions

D.W.: lead author; data analysis. M.R.: interpretation of results; manuscript development and refinement. S.W.: project design and management; interpretation of results.

Correspondence

Correspondence and requests for materials should be addressed to sw121@iu.edu.

Declaration of Interests

The authors declare no competing interests.